REVISTA MATÉRIA V.27 N.02
ISSN 1517-7076 artigos e13201, 2022

Evaluating the effect of autoclave curing on the microstructure and compressive strength evaluation of a high strength concrete

Dayana Cristina Silva Garcia[1,2], Karla Ulisses Lima[1], Kejin Wang[3], Roberto Braga Figueiredo[2]

[1]Department of Materials Engineering and Civil Construction, Universidade Federal de Minas Gerais, Av. Presidente Antônio Carlos, 6627, CP: 31270-901, Pampulha, Belo Horizonte, MG, Brazil.
[2]Department of Metallurgical Engineering, Universidade Federal de Minas Gerais, Av. Presidente Antônio Carlos, 6627, Pampulha, CP. 31270-901, Belo Horizonte, MG, Brazil.
[3]Department of Civil, Construction and Environmental Engineering, Iowa State University, Ames, IA 50011, USA.
e-mail: dayanacsgarcia@ufmg.br, karla.lima@ifnmg.edu.br, kejinw@iastate.edu, figueiredo@demet.ufmg.br

ABSTRACT

High strength concrete is usually cast with low water-to-binder ratio (w/b) in order to produce a compact microstructure with high strength and durability. Autoclave curing can accelerate cement hydration and pozzolanic reactions and further modify microstructure of cement pastes (such as decreasing the Ca/Si ratio and forming crystallized calcium silicate hydrate). The present paper evaluates the effect of w/b ratio, in the range 0.20 – 0.40, on compressive strength, porosity and microstructure of a high strength concrete. Some samples were subjected to autoclave curing in order to evaluate the effect of this process on the parameters evaluated. The microstructure was evaluated using X-ray diffraction and scanning electron microscopy. The results show the porosity decreased when w/b ratio decreased from 0.40 to 0.30 and thereafter the total porosity remained virtually constant while the water permeable porosity increased. An inverse relationship is observed between the porosity and the compressive strength. Autoclave curing affects significantly the phases developed in hardened concrete. It accelerates hydration and pozzolanic reactions, affects the interfacial transition zone and triggers the formation of crystalline C-S-H. These changes reflect in improved compressive strength at a low w/b but its effect is negligible at moderate w/b ratios.

Keywords: Calcium silicate hydrate, Autoclave curing, UHPC, Quartz flour; Compressive strength and porosity.

1. INTRODUCTION

High strength concrete (HSC) is often composed of large amounts of powder materials and a low water-to-binder ratio (w/b ≤0.35), which results in a compacted microstructure that provides the concrete with high density, high strength, and very low permeability [1]. However, as the w/b is further reduced, the density of concrete becomes difficult to be further improved due to insufficient workability. In addition, homogeneity of concrete microstructure becomes more critical in controlling the concrete properties. Therefore, to achieve ultra-high performance concrete (UHPC), a combined approach of using a very low w/b (≤0.20), effective superplasticizer, and various supplementary cementitious materials (SCMs) is generally employed to form a well packed system (commonly with elimination of coarse aggregates and sometimes addition of steel fibers). With the further improved density and homogeneity, UHPC possesses outstanding mechanical properties and durability [2, 3]. Concrete research and practice have shown that HSC uses silica fume and/or other pozzolanic materials at content lower than 10% by mass of Portland cement, while UHPC uses those materials at content higher than 20% [4, 5].

The improved homogeneity and density of HSC and UHPC result from uniform cement hydration, pozzolanic reaction, extreme low porosity, and very compact interfacial transitional zone between aggregate and binder matrix [6]. Although the overall microstructures of HSC and UHPC are significantly denser and homogenous, some entrained or entrapped air pores can develop in cement matrix [7]. Anhydrous phases are commonly observed due to a low w/b [8]. The main hydration products are calcium silicate hydrate (C-S-H), calcium hydroxide and ettringite crystals. Additionally, crystalline C-S-H phases can be formed under hydrothermal conditions [9]. Thus, the microstructure of UHPC is composed by residual cement grains, hydration products, aggregates and pores. The porosity may be reduced with aging because pores produced by air en-

Autor Responsável: Dayana Cristina Silva Garcia Data de envio: 10/02/2021 Data de aceite: 15/02/2022

10.1590/S1517-707620220002.1301

trapment are partially filled by calcium hydroxide and ettringite crystals in standard cured samples. Autoclave cured samples can have pores filled by crystalline C-S-H phases [10, 11]. Although the total porosity of UHPC is generally only about 2%, this porosity can be further reduced when the concrete is cured at an elevated temperature (150 - 200°C). The strength development of the concrete could be further accelerated with steam curing or autoclave curing [12, 13].

In the precast concrete industry, heat treatment is often used to accelerate cement hydration and improve early age mechanical property development so as to improve concrete productivity [14]. Heat treatment is usually employed in UHPC after the final setting time at temperatures in the range 90 ~ 220 °C [11, 15-17]. A recent paper [18] reported the investigation of the effect of five types of curing regimes on the mechanical properties, nanomechanical and microstructure of UHPC. It was found that the concretes subjected to autoclave curing exhibited the higher gain in strength. It has been shown that under autoclave curing, the Ca/Si ratio decreases with increasing of Si-rich materials which increases the compressive strength [11]. In addition, under hydrothermal conditions, the utilization of pozzolanic materials is preferred since those materials react with calcium hydroxide produced from cement hydration, form additional C-S-H gel, and prevent the formation of crystalline phase α-C2SH [$Ca_2SiO_3(OH)_2$] [19-21]. The formation of α-C_2SH is considered prejudicial since it is responsible for the solid volume reduction in concrete, which in turn produces pores, increase concrete permeability, and decrease concrete mechanical properties [22, 23]. However, in the presence of quartz flour, and temperature in the range 170 °C–220 °C, calcium silicate hydrate can convert in crystalline 11Å tobermorite and xonotlite, and the formation of those phases is favored for strength development [11, 24-26].

It is known that C-S-H system is highly complex with several phases reported. The C-S-H system presents metastable crystalline phases (Z-phase), crystalline stable phases and poorly order gel such as C-S-H gel [22]. The C-S-H is the main product of Portland cement hydration and when the hydration process happens at room temperature it is poorly crystalline and with variable Ca/Si ratio (0.6-2.0) [27]. There are more than 30 stable phases with different Ca/Si ratio and a summary is available in the literature [22, 24]. The most common forms of crystallized calcium silicate hydrate are tobermorite [$Ca_5(OH)_2Si_6O_{16}.4H_2O$; Ca/Si = 0.83] and xonotlite [$Ca_6(Si_6O_{17})(OH)_2$; Ca/Si = 1.0] [29]. Xonotlite forms at high temperatures than tobermorite. Additionally, tobermorite and xonotlite can be identified by their morphology since the former appears as platy-like and the latter as needle-like structures [30].

The performance of concrete is directly influenced by the concrete microstructure, where w/b plays an important role as it defines the concrete porosity. In addition, crystalline hydration products, such as ettringite and porlandite, preferably form in large pores, and their morphology changes in the pastes with different w/b [31]. For UHPC, where w/b ratio is lower than 0.20, homogeneous microstructure of the concrete is also achieved by use of high silica fume and superplasticizer content and employment of pressure during early age curing (before setting) [32]. Since superplasticizer effectively improves workability [33], it also permits to use very little water in UHPC, thus limiting cement hydration and resulting in changes in the concrete microstructure. Existing research has focused extensively on the effects of w/b on concrete mechanical and transport properties, the latter of which controls by concrete pore structure. However, the effect of autoclave curing on microstructure of concrete with low w/b ratio is not very clear. It is expected that the high temperature and pressure will affect pore structure and hydration products. Thus, the aim of the present work is to investigate the influence of autoclave curing on the microstructure of concrete with low and very low w/b. The microstructures of the concretes are characterized using X-ray diffraction (XRD) and scanning electrical microscope (SEM). The compressive strength and porosity of the concretes are also studied. The detailed experimental work and test results are reported as below.

2. MATERIALS AND METHODS

The concrete samples were prepared with the following materials: (1) Ordinary Portland Cement (OPC) containing up to 5% limestone filler, (2) amorphous white silica fume (SF), (3) crystalline ground quartz flour (QF), (4) river sand with the maximum size of 600 µm, and (5) polycarboxylate based superplasticizer (35% solids content, pH 7,5 and density of 1,1 g/cm³). The chemical compositions, determined by x-ray fluorescence, and specific gravity of the dry materials used in this investigation are listed in the Table 1. Figure 1 shows their particle size distribution. Details on the chemical composition and particle size distribution of the particular materials (OPC, SF, QF, and sand) are also reported elsewhere [26, 34].

Table 1: Chemical composition (wt. %) of the OPC, silica fume and ground quartz flour

Material	SiO_2	CaO	Al_2O_3	Fe_2O_3	MgO	TiO_2	P_2O_5	LOI	Specific gravity, $g.cm^{-3}$
OPC	24.59	56.47	7.90	4.05	2.43	0.25	0.12	3.5	3.17
Silica Fume	94.70	0.97	0.24	0.07	1.29	0.03	0.09	2.81	2.18
Gound Quartz flour	96.0	-	-	-	-	-	-	-	2.68

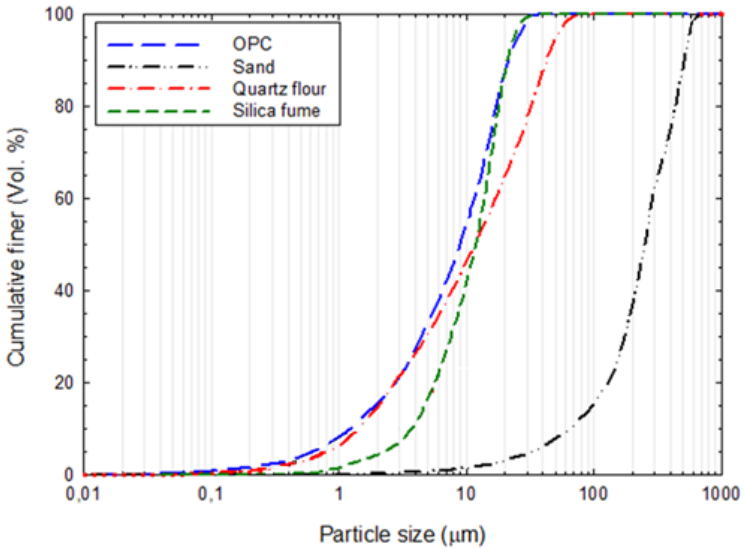

Figure 1: Particle size distribution of the raw materials

In this study, the proportion of all particular materials was determined based on the maximum particle packing density theory. To determine the proportion, the modified Andreasen and Andersen model [35] was used as a target function, and the proportion of each material was adjusted for the optimal approximation between the target curved and the composed mixture. The optimization was based on the Least Squares Method (LSM). When the results were minimized, the composition of the concrete was treated as the best one. Since the particular materials used in this study is rich in fines, the distribution modulus q adopted was 0.23 as recommended by YU *et al.* [36]. The optimal proportion of these particular materials was OPC:SF:QF:sand =1:0.25: 0.20:1.0, where the LSM is 1224. The w/b used ranged from 0.20 to 0.40 with increments of 0.05. The amount of superplasticizer was determined by means of the flow table test, in which the flow diameter was kept constant at 200 ± 20 mm. The proportion of each mix is listed in Table 2.

Table 2: Mixture proportions of concretes with different w/b ratio (kg/m^3)

Mix ID	Binder		Sand (kg/m^3)	Quartz flour (kg/m^3)	Water (w/b) (kg/m^3)	Superplasticizer (wt. % of binder)
	OPC (kg/m^3)	Silica fume (kg/m^3)				
1	724	181.0	724	144.8	362.0 (0.40)	0.25
2	758	189.5	758	151.6	331.6 (0.35)	0.50
3	795	198.8	795	159.0	298.1 (0.30)	1.00
4	837	209.3	837	167.4	261.6 (0.25)	1.50
5	883	220.8	883	176.6	220.8 (0.20)	2.00

The concrete was mixed in a Hobart mixer with a total mixing time of 15 minutes. The mixing sequence was as follows: the powder materials were dry-mixed in the mixer at a speed of 185 rpm during 3 minutes. Then, a half of the designed water and superplasticizer was put into the pre-mixed powder and mixed for more 3 minutes. Next, the remaining water and superplasticizer was added to the mixer incrementally and further mixing for 15 minutes until the mixture flows [21]. The freshly mixed concrete was placed in steel cubic molds (40x40x40 mm³), and vibrated using a vibrating table for 30 seconds. After casting, all samples were covered and stored in a curing room (25°C and 95% RH) for 24 hours prior to demolding. Then, two different curing regimes were used: (1) conventional curing: 25°C and 95% RH until testing; (2) autoclave treatment: temperature and pressure gradually increased for 2 hours to 220 °C and 2.1 atm, holding time of 8 hours, slow curing to room temperature (inside the autoclave) and then the samples were stored at 25°C and 95% RH until testing. It has been shown that, under hydrothermal conditions and temperature around 220 °C the quartz flour becomes chemically reactive [26, 37].

Both the compressive strength and the porosity were determined at 7 and 28 days and at least four samples were tested at each age to compute the average. The total porosity and the water permeable porosity were measured applying the vacuum-saturation technique based on Archimedes principle. The total porosity and the water permeable porosity were calculated from the following equations, respectively [36].

$$P_T = 100x\left[1-\left(\frac{m_d}{\rho(m_s - m_w)}\right)\right] \quad (1)$$

$$\phi_{V,\,water} = \frac{m_s - m_d}{m_s - m_w} \cdot 100 \quad (2)$$

Where: PT is the total porosity (%), md is the mass of oven dried sample (g), ρ is theoretical density of the material (g/cm³), ms is the mass of saturated samples in surface-dry condition measured in air (g), mw is the mass of water-saturated sample in water (g) and ϕv, water is the water permeable porosity (%).It is worth mentioning that theoretical density is based on starting compositions of the samples following pure component densities.

The phases present in each sample were determined using X-ray diffraction. Samples were ground and particles smaller than 63 μm were used for the characterization. The diffraction patterns were recorded with a Philips-PANalytical Empyrean diffractometer using monochromatic CuKα radiation (λ = 1,5406 A) over the 2θ range from 3° to 50°, step size of 0.03 and count time of 3 seconds. Also, the surface of fractured specimen pieces were observed using secondary electrons in a scanning electron microscope. The pieces were coated with ~15 nm thick carbon layer to enhance conductivity. The micrographs were recorded using a Quanta FEG 3D FEI field emission gun scanning electron microscope (FEG-SEM) equipped with energy-dispersive X-ray spectroscopy (EDS). The FEG-SEM operating conditions were 5 kV accelerating voltage and 10 mm work distance.

3. RESULTS

3.1 Compressive strength and porosity

Figure 2 shows the compressive strengths, after 7 days and after 28 days, of the concrete samples prepared with different w/b and subjected to standard curing regime and autoclave treatment. The results show that decreasing w/b from 0.40 to 0.35 increases the strength in samples subjected to conventional curing. The strength does not change significantly with further decrease in w/b ratio and, in fact, a slight decrease was observed in the minimum w/b ratio of 0.20. The samples subjected to autoclave curing display increase in strength with decreasing w/b ratio down to 0.30. The strength at lower w/b ratio is similar for samples cured 7 days but a slight decrease, with decreasing w/b ratio, is observed for samples cured 28 days. Compressive strengths over 80 MPa are observed in conventional cured samples with w/b ratio between 0.25 and 0.35. Autoclave treatment in samples with w/b ratio of 0.25 and 0.30 increases the compressive strength to over 100 MPa.

Figure 3 shows the total and water permeable porosity of the different samples. The results show a tendency of decreasing porosity when the w/b ratio decreased from 0.40 to 0.30. There is no significant change in total porosity with further decrease in w/b ratio but a slight increase in water permeable porosity is noticed. As expected, there is a trend of decreasing porosity with increasing curing time.

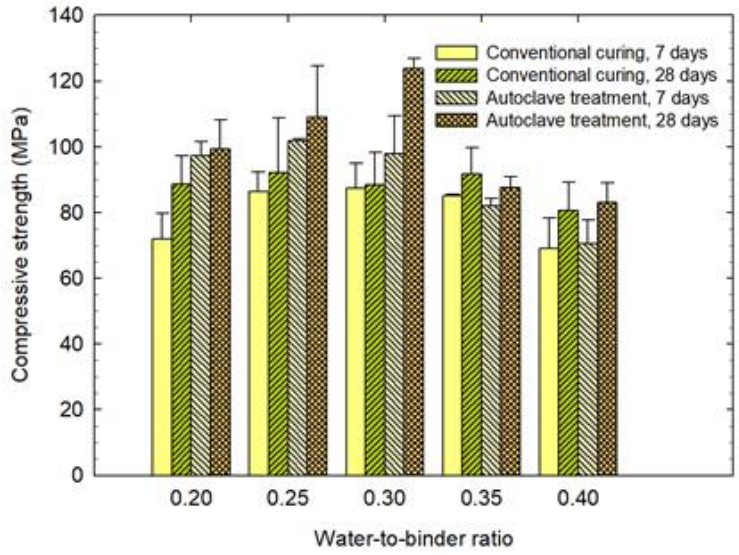

Figure 2: Influence of the w/b ratio and curing procedure on the mechanical properties of the concrete with conventional curing and autoclave curing

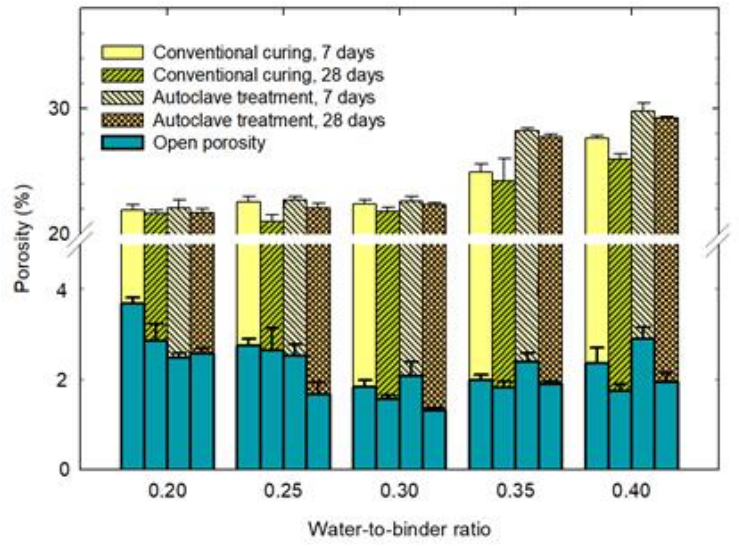

Figure 3: Influence of the w/b ratio and curing procedure on the total porosity and the water permeable porosity of the concrete with conventional curing and autoclave curing

3.2 Microstructure

The results of qualitative phase assessment by X-ray diffraction are presented in Figure 4. Principal crystalline phases in the concrete cured at room temperature are quartz, ettringite, calcium hydroxide and the anhydrous phases alite and belite (Figure 4 a). Additionally, semi-crystalline calcium silicate hydrate (C-S-H) is expected in concrete. Peaks characteristic of ettringite are located at $2\theta \approx 9.1°$ and 15.8°; and portlandite from the peaks at ~18.1° and ~34.1°. Furthermore, peaks characteristic of a semi-crystalline C-S-H are located at $2\theta \approx 29.3°$ - 30.7° and 31.8° [27, 38]. In addition, the data shows a decrease of the intensity of peaks of calcium hydroxide and rise of the peaks of alite and belite as the w/b decreased. This suggests an increase of the volume of anhydrous phases and a decrease of hydration product which is associated with a decrease in hydration kinetics. Figure 4 (b) shows that calcium hydroxide and ettringite were not detected in samples subjected to autoclave curing. Also, the intensity of the peaks associated with anhydrous phases decreased suggesting an increase in hydration kinetics. Crystalline phases tobermorite and xonotlite were observed in the samples with higher w/b ratio cured in autoclave. The main 11 Å tobermorite peak is at the diffraction angle of 7.76°, while a shouldered peak at $2\theta \approx 28.84°$ and a peak at $2\theta \approx 27.47°$ indicate the formation of xonotlite.

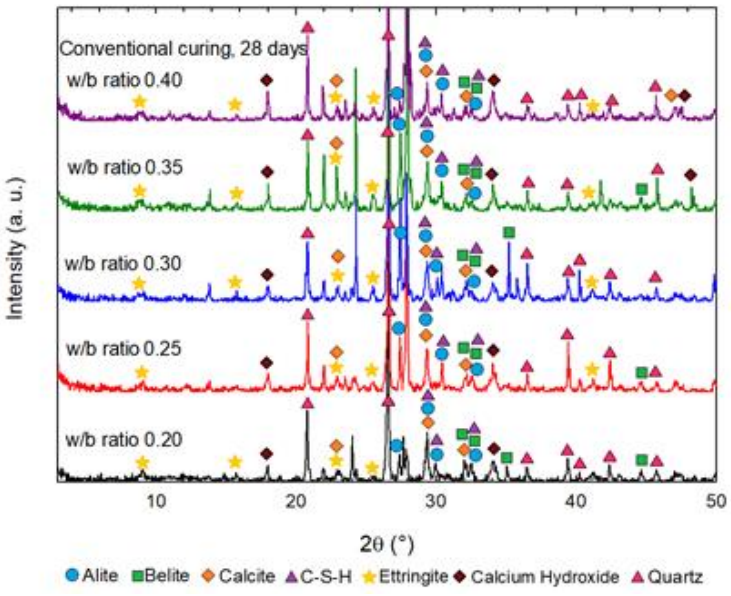

(a)

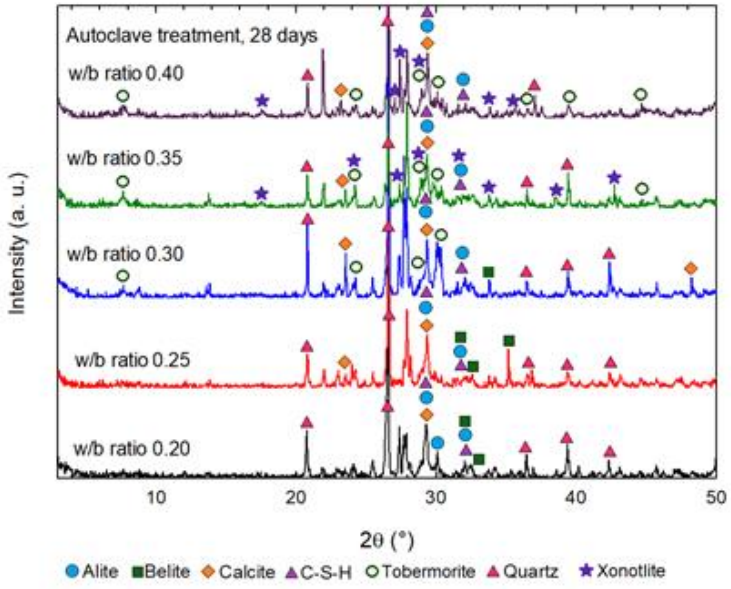

(b)

Figure 4: Diffractograms of the concretes with (a) conventional curing and (b) with autoclave treatment

Figure 5 shows low magnification images of the surface of fractured samples of all conditions tested. Thus, all the concrete exhibited a dense microstructure with sand particles and some visible pores. The amount of visible pores in Figure 5 was larger in the sample with w/b ≈ 0.40 and autoclave curing. Although a pore with 400 µm diameter was observed, the pore sizes are around 50 µm. There was no significant variation, at this magnification, between the microstructures of the samples with conventional curing or autoclave treatment. However, the morphology of the hydration products, the interfacial transition zone and some spherical features displayed differences when observed at higher magnification.

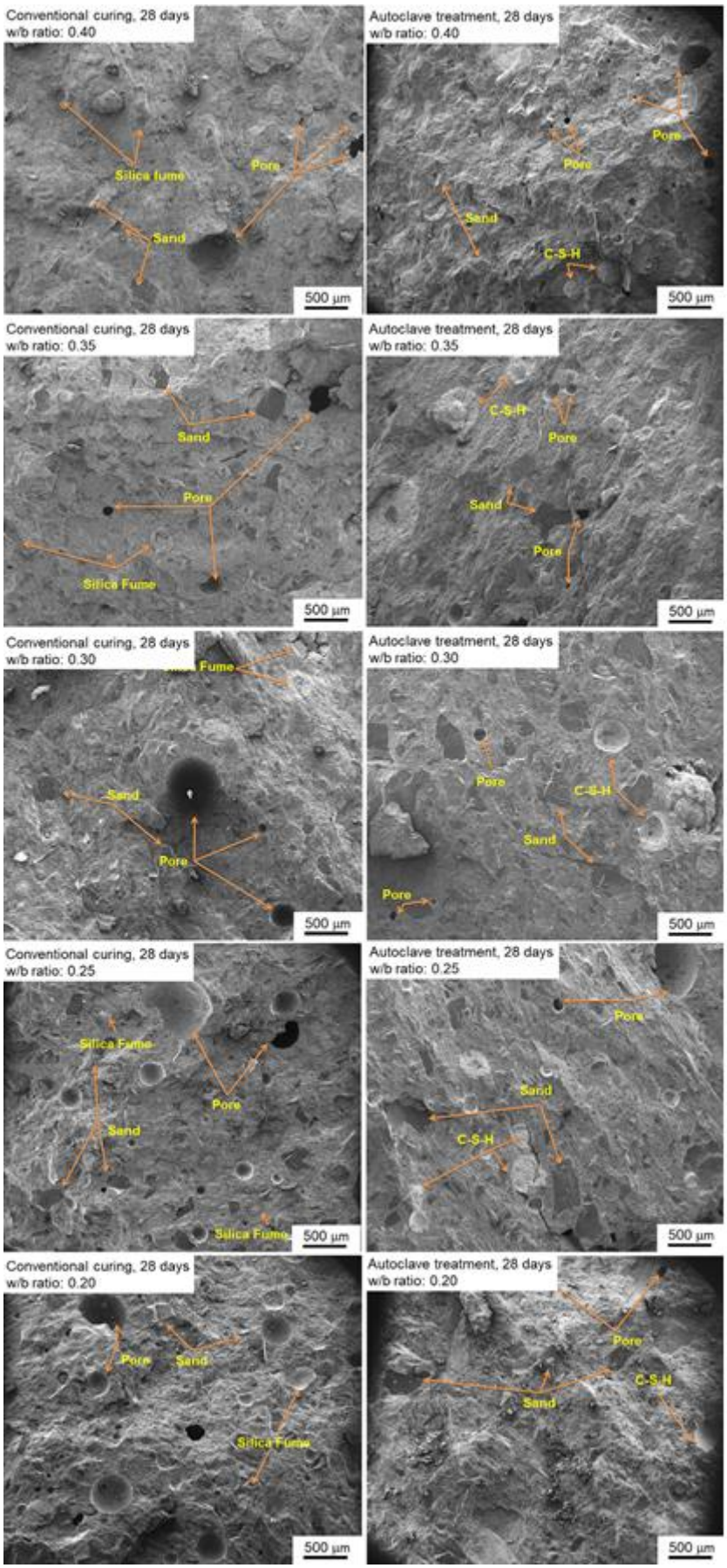

Figure 5: SEM images of hardened paste in the concretes

Figure 6 shows details of the spherical structures and their chemical composition in a sample subjected to conventional curing and one with autoclave curing. The conventional cured sample exhibited agglomeration of silica fume which is characterized by rounded shape with some cracks and exhibits spherical particles rich in Si. The autoclave cured concrete presents platy-like crystals which are characteristic of tobermorite phase [25, 30, 39]. It is worth noting that this phase was also identified by XRD. Figure 7 shows images of the interfacial transition zone (ITZ) for the samples with the highest and minimum w/b ratio. A thin discontinuity is observed in the conventional cured samples while the autoclave cured samples display a continuous transition from the sand particles into the concrete matrix.

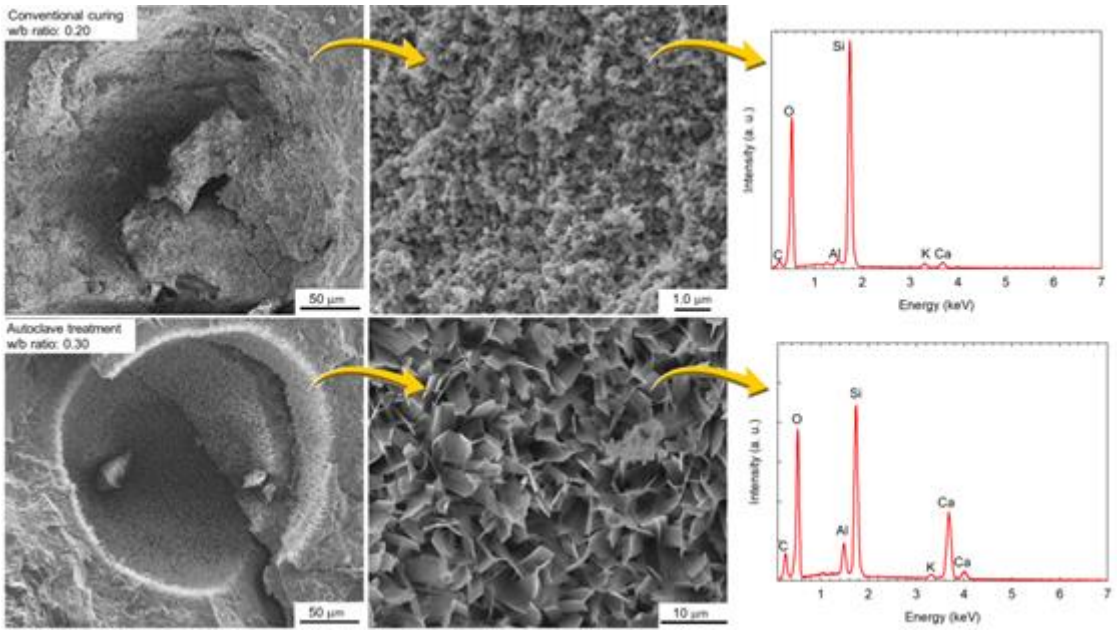

Figure 6: SEM images and EDS analysis of the silica fume and calcium silicate hydrate

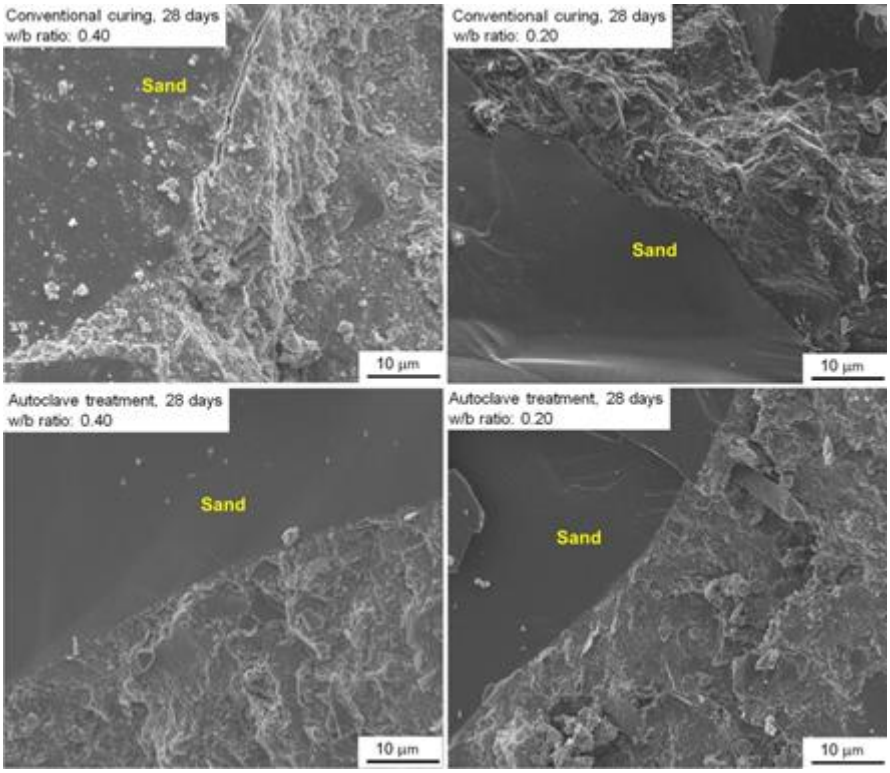

Figure 7: SEM images of the interfacial transition zone

Observations at high magnification inside the pores of the different samples enabled the identification of multiple phases due to their morphology. Figure 8 shows representative images of some of the features. Thus, in the conventional cured samples the air bubbles were filled with big and well-developed hexagonal plates which are typically associated with calcium hydroxide crystals. These samples also contained prismatic, thin, needle-like features which were associated with ettringite crystals. Sponge-like material behind the calcium hydroxide and the ettringite crystals are associated with C-S-H. Crystalline platy-like and needle-like structures characteristic of tobermorite and xonotlite were observed in the sample subjected to autoclave curing. Furthermore, an unusual structure was found in the concrete prepared with w/b of 0.30 and autoclave curing. This structure is rich in Si and appears as a spherical aggregate of thin blades.

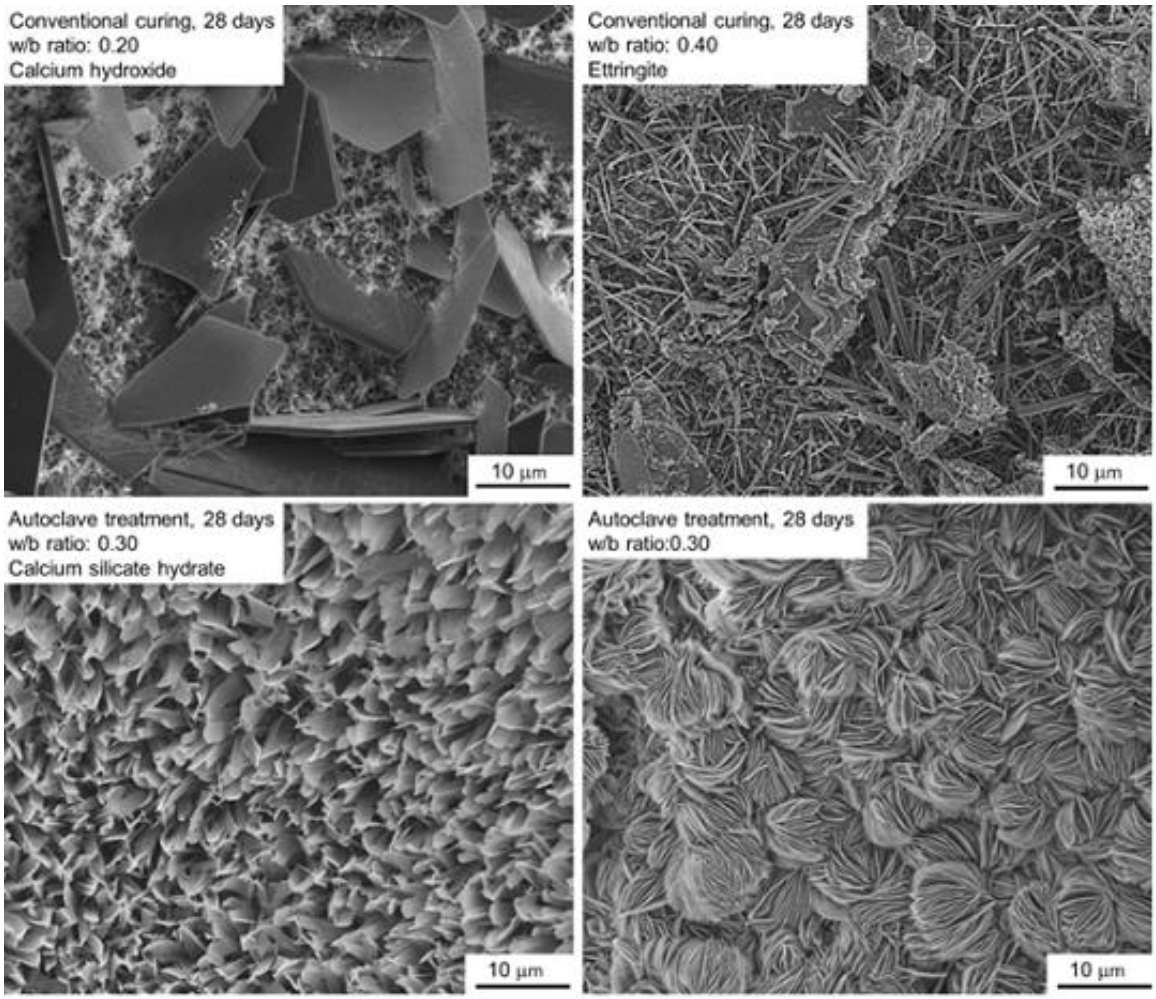

Figure 8: SEM images of (a) calcium hydroxide, (b) ettringite, (c) crystalline calcium silicate hydrate and (d) a spherical aggregate of thin blades

4. DISCUSSION

4.1 Effect of w/b ratio in conventional cured concrete

It is known that - w/b - affects the cement hydration [40], porosity and compressive strength in concrete. Reducing w/b usually results in lower porosity [6, 17] and higher compressive strength. This trend is observed in the present results for the w/b ratio range 0.30 ~ 0.40, except for the compressive strength at 28 days of the sample conventionally cured which did not increase from 0.35 to 0.30. This trend is not observed in the samples with a lower w/b. This disagreement is attributed to the casting procedure. It is known that casting without pressure can lead to high porosity [41]. The samples were not subjected to pressure casting in the present experiments and there was no significant change in total porosity with decreasing w/b ratio from 0.30 to 0.20.

In fact there was an increase in open porosity in this range.

It is known that compressive strength is influenced by the ITZ and matrix porosity and there is a direct relationship between the mechanical properties and the w/b ratio [42]. However, when w/b is lower than 0.30, the ITZ becomes dense and thin and the matrix porosity plays a major role. Consequently, any amount of air void results in a considerable reduction of compressive strength [43]. SEM showed the ITZ was dense, without significant porosity, microcracks nor calcium hydroxide. Also SEM showed evidence of pores in all samples regardless of w/b ratio. This explains the reduced compressive strength in samples with very low w/b ratio.

The porosity of hardened concrete can also be affected by the rheological behavior in the fresh state. The rheology behavior can be described with at least two parameters, yield stress and plastic viscosity [44, 45] although only one parameter is usually determined [46]. In the present study, flow table test was used to analyze the flowability of the concrete, and this test evaluates the yield stress, the minimum stress required for initiating a flow. Two concretes can have the same slump value, or the same yield stress, but different plastic viscosity [47]. In addition, a concrete mixture composed of a high amount of powder materials and low water content usually presents a high plastic viscosity [44]. In the concretes with a high slump, the plastic viscosity plays an important role in characterizing the concrete consistency. Also, the influence of paste volume, w/b ratio, and the amount of superplasticizer on the rheological parameters becomes smaller as the w/b ratio increases [44]. It is difficult to cast and to eliminate air voids if concrete has a high plastic viscosity, even in situations where the yield stress is within the desired range and with the aid of vibration, due to a sticky aspect [46]. This difficulty arises from the plastic viscosity as it is a consequence of surface contacts and friction between the particles. Due to the high superficial surface area of the materials in the concrete, it is necessary to have more paste to decrease the particle friction [48]. Also, spherical air pores can be formed as a side effect of high amount of superplasticizer [10]. Therefore, the inability to decrease porosity in samples with a w/b ratio below 0.30 is partially attributed to the viscosity of the concrete in the fresh state and the increased amount of superplasticizer.

4.2 Effect of autoclave curing

The XRD pattern of conventionally cured concrete showed evidence of calcium hydroxide and ettringite, and these phases were clearly observed in large pores by SEM. It is expected that calcium hydroxide does not contribute to improving the mechanical properties due to their weak adhesion to the matrix and because they are preferred cleavage sites [43]. Also, careful examination by SEM has evidenced unreacted silica fume agglomerations in the conventionally cured concrete samples (Fig. 5) due to the difficulty of dispersion. These agglomerations may also compromise the mechanical properties of the concrete [34]. On the other hand, the samples subjected to autoclave treatment do not show evidence of calcium hydroxide. Si-rich concretes can undergo pozzolanic reactions under hydrothermal conditions, consuming the calcium hydroxide. In this case, both silica fume and quartz flour react with calcium hydroxide and produce additional C-S-H [26, 49]. Also, the hydration kinetics is accelerated under hydrothermal conditions [16, 50]. Both effects are expected to improve strength. Other evidence of pozzolanic reaction, in autoclave cured samples, is the absence of α-C_2SH [51, 52]. In addition, crystals of calcium silicate hydrate were observed in the pores of the concrete submitted to autoclave treatment.

These changes in phases developed during the different curing regimes are expected to affect the compressive strength. Thus, the autoclaved concrete was expected to display higher strength due to the pozzolanic reactions, acceleration of hydration and formation of crystalline C-S-H. In fact, the samples with w/b ratio of 0.30 and lower, subjected to autoclave curing, exhibited an increase in strength when compared to the conventionally cured samples. It is important to note that the increase in strength due to autoclave treatment was not related to a decrease in porosity. It is attributed to the changes in structure and in the ITZ which becomes denser and continuous. On the other hand, autoclave curing did not change the strength of samples with w/b ratio of 0.35 and 0.40. These samples exhibited the larger amount of total porosity and the limited strength is attributed to this. It was the opposite of expected; the autoclave treatment leads to decreased porosity and pore size of UHPC [18, 21].

The sample with w/b of 0.30 and autoclave curing displayed areas covered with spherical aggregates of thin lamellas. This morphology is comparable to gyrolite [53]. Gyrolite presents molar Ca/Si ratio of 0.66 and water/solid ratio of 10 and it can be formed in temperature higher than 120°C under hydrothermal conditions [23]. However, the formation of gyrolite is slow [22], in conditions similar to the present study. Traces of gyrolite were found in suspensions prepared with molar Ca/Si ratio of 0.66 and with the addition of gypsum after 8 hours under hydrothermal conditions (200°C under the saturated steam pressure) [54].

5. SUMMARY AND CONCLUSIONS

Concrete samples were prepared with different water/binder ratio (0.2-0.40) and subjected to conventional and autoclave curing. The compressive strength and porosity of the different samples were determined and microstructures were characterized using XRD and SEM. The results lead to the following conclusions.

The total porosity decreases with decreasing w/b from 0.40 to 0.30, and this is associated with an increase in strength. Further decrease in w/b did not change the total porosity and did not increase the strength of the concrete. The porosity at a very low w/b ratio is associated with entrapped air, which is possibly attributed to the viscosity of the concrete in the fresh state and the increased amount of superplasticizer.

Autoclave curing promotes pozzolanic reactions, which disintegrates unreacted silica fume agglomerates and eliminates calcium silicate, induces crystallization of C-S-H and produces a continuous ITZ. These microstructural changes improve the concrete strength at a low w/b ratio but are not effective in samples with w/b larger than 0.30 due to the high porosity in these conditions.

6. ACKNOWLEDGMENTS

The authors acknowledge the financial support from FAPEMIG, CNPq, CAPES and the Microscopy Center of UFMG for SEM experiments.

7. REFERENCES

[1] SONG, P.S., HWANG, S., "Mechanical properties of high-strength steel fiber-reinforced concrete", *Construction and Building Materials*, v. 18, pp.669–73, 2004.

[2] TUAN, N.V., YE, G., BREUGEL, K.V., *et al.* "Hydration and microstructure of ultra high performance concrete incorporating rice husk ash", *Cement and Concrete Research*, v. 41, pp.1104-11, 2011.

[3] LESSLY, S.H., KUMAR, S.L., JAWAHAR, R.R., *et al.* "Durability properties of modified ultra-high performance concrete with varying cement content and curing regime", *Materials Today: proceedings*, v. 45, pp.6426-32, 2021.

[4] ARORA, A., AGUAYO M., HANSEN H., *et al.* "Microstructural packing- and rheology-based binder selection and characterization for Ultra-high Performance Concrete (UHPC)", *Cement and Concrete Research*, v. 103, pp.179–90, 2018.

[5] SCHIAVON, J.Z., BORGES, P.M., SILVA, S.R.D., *et al.* "Analysis of mechanical and microstructural properties of high performance concretes containing nanosilica and silica fume", *Matéria*, v. 26, 2021.

[6] SCHRÖFL, C., GRUBER, M., PLANK, J., "Preferential adsorption of polycarboxylate superplasticizers on cement and silica fume in ultra-high performance concrete (UHPC) ", *Cement and Concrete Research*, v. 42, pp.1401-8, 2012.

[7] YAZICI, H., YARDIMCI, M. Y., KARABULUT A.S., *et al.* "Mechanical properties of reactive powder concrete containing mineral admixtures under different curing regimes", *Construction and Building Materials*, v. 23, pp.1223-31, 2009.

[8] HE, Z.-H., DU, S.-G., CHEN, D., "Microstructure of ultra high performance concrete containing lithium slag", Journal of Hazardous Materials, v. 353, pp.35-43, 2018.

[9] ALHOZAIMY, A., JAAFAR M.S., AL-NEGHEIMISH A., *et al.* "Properties of high strength concrete using white and dune sands under normal and autoclaved curing", *Construction and Building Materials*, v. 27, pp.218-22, 2012.

[10] YAZıCı, H., YIGITER H., KARABULUT A.S., *et al.* "Utilization of fly ash and ground granulated blast furnace slag as an alternative silica source in reactive powder concrete", *Fuel*, v. 87, pp.2401–7, 2008.

[11] YAZıCı, H., DENIZ E., BARADAN B., "The effect of autoclave pressure, temperature and duration time on mechanical properties of reactive powder concrete", *Construction and Building Materials*, v. 42, pp.53-63, 2013.

[12] WANG, D., SHI, C., WU, Z., *et al.* "A review on ultra high performance concrete: Part II. Hydration, microstructure and properties", *Construction and Building Materials*, v. 96, pp.368–77, 2015.

[13] LUO, B., LUO Z., "Influence of curing regimes on the mechanical properties and microstructure of ultra-high-performance concrete blended with gold mine tailings", *Materials Letters*, v. 311, pp.131527, 2022.

[14] CWIRZEN, A., "The effect of the heat-treatment regime on the properties of reactive powder concrete", *Advances in Cement Research*, v. 19, pp.25-33, 2007.

[15] COURTIAL, M., NOIRFONTAINE M.N.D., DUNSTETTER F., *et al.* "Effect of polycarboxylate and crushed quartz in UHPC: microstructural investigation", *Construction and Building Materials*, v. 44, pp.699-705, 2013.

[16] CHEYREZY, M., MARET, V., FROUIN, L., "Microstructural analysis of RPC (reactive powder concrete)", *Cement and Concrete Research*, v. 25, pp.1491-500, 1995.

[17] SHI, C., WU, Z., XIAO, J., *et al.*"A review on ultra high performance concrete: Part I. Raw materials and mixture design", *Construction and Building Materials*, v. 101, pp.741–51, 2015.

[18] SHEN, P., LU, L., HE, Y., *et al.*"The effect of curing regimes on the mechanical properties, nano-mechanical properties and microstructure of ultra-high performance concrete", *Cement and Concrete Research*, v. 118, pp.1-13, 2019.
[19] HONG, S.-Y., GLASSER F.P., "Phase relations in the $CaO–SiO_2–H_2O$ system to 200ºC at saturated steam pressure", *Cement and Concrete Research*, v. 34, pp.1529-34, 2004.
[20] ESCALANTE-GARCIA, J.I., SHARP, J.H., "Effect of the temperature on the hydration of the main clinker phase in Portland cements: part II, blended cements", *Cement and Concrete Research*, v. 28, pp.1259-74, 1998.
[21] CHEN, T., GAO, X., REN, M., "Effects of autoclave curing and fly ash on mechanical properties of ultra-high performance concrete", *Construction and Building Materials*, v. 158, pp.864–72, 2018.
[22] MELLER, N., HALL, C., KYRITSIS, K., *et al.* "Synthesis of cement based $CaO–Al_2O_3–SiO_2–H_2O$ (CASH) hydroceramics at 200 and 250 °C: Ex-situ and in-situ diffraction", *Cement and Concrete Research*, v. 37, pp.823-33, 2007.
[23] LUKE, K., "Phase studies of pozzolanic stabilized calcium silicate hydrates at 180 °C ", *Cement and Concrete Research*, v. 34, pp.1725-32, 2004.
[24] RICHARDSON, I.G., "The calcium silicate hydrates", *Cement and Concrete Research*, v. 38, pp.137-58, 2008.
[25] TAM, C.-M., TAM V.W.-Y., "Microstructural behaviour of reactive powder concrete under different heating regimes", *Magazine of Concrete Research*, v. 64, pp.259-67, 2012.
[26] GARCIA, D.C.S., WANG, K., FIGUEIREDO, R.B., "The influences of quartz content and water-to-binder ratio on the microstructure and hardness of autoclaved Portland cement pastes", *Cement and Concrete Composites*, v. 91, pp.138–47, 2018.
[27] KUNTHER, W., FERREIRO, S., SKIBSTED, J., "Influence of the Ca/Si ratio on the compressive strength of cementitious calcium–silicate–hydrate binders", *Journal of Materials Chemistry* A, v. 5, pp.17401-12, 2017.
[28] SHAW, S., CLARK S.M., HENDERSON C.M.B., "Hydrothermal formation of the calcium silicate hydrates, tobermorite ($Ca_5Si_6O_{16}(OH).4H_2O$) and xonotlite (Ca6Si6O17(OH)2): an in situ synchrotron study.", *Chemical Geology*, v. 167, pp.129-40, 2000.
[29] BLACK, L., GARBEV, K., STUMM, A., "Structure, bonding and morphology of hydrothermally synthesized xonotlite", *Advances in Applied Ceramics*, v., 2013.
[30] ZHAO, Y., ZHANG, Y., CHEN, T., *et al.* "Preparation of high strength autoclaved bricks from hematite tailings", *Construction and Building Materials*, v. 28, pp.450-5, 2012.
[31] NIU, D., WANG, J., WANG, Y., "Effect of hydration aging and water binder ratio on microstructure and mechanical properties of sprayed concrete", *Journal of Wuhan University of Technology-Mater Sci E*d, v. 30, pp.745–51, 2015.
[32] WANG, C., YANG, C., LIU, F., *et al.* "Preparation of Ultra-High Performance Concrete with common technology and materials", *Cement and Concrete Composites*, v. 34, pp.538–44, 2012.
[33] MATOS, P.R.D., SAKATA, R.D., FOIATO M., *et al.* "Workability maintenance of water-reducing admixtures in high-performance pastes produced with different types of Portland cement", *Matéria*, v. 26, 2021.
[34] GARCIA, D.C.S., SOARES M.M.N.D.S., BEZERRA, A.C.D.S., *et al.*"Microstructure and hardness of cement pastes with mineral admixture", *Matéria*, v. 22, pp.1-10, 2017.
[35] ANDREASEN, A. H. M., ANDERSEN J., "Ueber die Beziehung zwischen Kornabstufung und Zwischenraum in Produkten aus losen Körnern", *Kolloid-Zeitschrift*, v. 50, pp.217-28, 1930.
[36] YU, R., SPIESZ P., BROUWERS H. J. H., "Mix design and properties assessment of Ultra-High Performance Fiber Reinforced Concrete (UHPFRC)", *Cement and Concrete Research*, v. 56, pp.29-39, 2014.
[37] CONSTANTINO, J.C.P., GARCIA D.C.S., PALHARES H.G., *et al.* "Development of functional TiO_2 coatings deposited on cementitious materials ", *Construction and Building Materials*, v. 250, 2020.
[38] KONTOLEONTOS, F., TSAKIRIDIS P., MARINOS A., *et al.* "Dry-grinded Ultrafine Cements Hydration. Physicochemical and Microstructural Characterization", *Materials Research*, v. 16, pp.404-16, 2013.
[39] MOSTAFA, N.Y., SHALTOUT A.A., OMAR H., *et al.* "Hydrothermal synthesis and characterization of aluminium and sulfate substituted 1.1 nm tobermorites", *Journal of Alloys and Compounds*, v. 467, pp.332-7, 2009.
[40] PEREIRA, M.M.L., SOUZA, A.L.R.D., CAPUZZO V.M.S., *et al.* "Effect of the water/binder ratio on the hydration process of Portland cement pastes with silica fume and metakaolin", *IBRACON Structures and Materials Journal*, v. 15, 2022.
[41] REDA, M.M., SHRIVE N.G., GILLOTT J.E., "Microstructural investigation of innovative UHPC", *Cement and Concrete Research*, v. 29, pp.323-239, 1999.
[42] YOO, D.-Y., BANTHIA N., "Mechanical properties of ultra-high-performance fiber-reinforced concrete: A review", *Cement and Concrete Composites*, v. 73, pp.267-80, 2016.
[43] MEHTA, P., MONTEIRO P.J.M. Concrete: Microstructure, Properties, and Materials. 3 ed: McGraw-Hill Education; 2006.
[44] WALLEVIK, O.H., WALLEVIK J.E., "Rheology as a tool in concrete science: The use of rheographs and workability boxes", *Cement and Concrete Research*, v. 41, pp.1279-88, 2011.
[45] WALLEVIK, J.E., "Rheological properties of cement paste: Thixotropic behavior and structural breakdown", *Cement and Concrete Research*, v. 39, pp.14-29, 2009.

[46] FERRARIS, C.F., "Measurement of the Rheological Properties of High Performance Concrete: State of the Art Report", *Journal of Research of the National Institute of Standards and Technology*, v. 104, pp.461-78, 1999.
[47] WALLEVIK, J.E., "Relationship between the Bingham parameters and slump", *Cement and Concrete Research*, v. 36, pp.1214-21, 2006.
[48] JIAO, D., SHI, C., YUAN, Q., *et al.* "Effect of constituents on rheological properties of fresh concrete-A review", *Cement and Concrete Composites*, v. 83, pp.146-59, 2017.
[49] ALAWAD, O.A., ALHOZAIMY, A., JAAFAR, M.S., *et al.*"Microstructure analyses of autoclaved ground dune sand–Portland cement paste", *Construction and Building Materials*, v. 65, pp.14-9, 2014.
[50] VAN, V.-T.-A., RÖßLER, C., BUI D.-D., *et al.* "Rice husk ash as both pozzolanic admixture and internal curing agent in ultra-high performance concrete", *Cement and Concrete Composites*, v. 53, pp.270–8, 2014.
[51] CAO, Y., DETWILERL R.J., "Backscattered electron imaging of cement pastes cured at elevated temperatures", *Cement and Concrete Research*, v. 25, pp.627-38, 1995.
[52] PATEL, H.H., BLAND, C.H., POOLE, A.B., "The microstructure of concrete cured at elevated temperatures", *Cement and Concrete Research*, v. 25, pp.485-90, 1995.
[53] RÓŻYCKA, A., KOTWICA, Ł., MAŁOLEPSZY, J., "Synthesis of single phase gyrolite in the CaO-quartz-Na2O-H2O system", *Materials Letters*, v. 120, pp.166-9, 2014.
[54] BALTAKYS, K., SIAUCIUNAS R., "Influence of gypsum additive on the gyrolite formation process", *Cement and Concrete Research*, v. 40, pp.376-83, 2010.

ORCID

Dayana Cristina Silva Garcia https://orcid.org/0000-0002-8572-5531
Karla Ulisses Lima https://orcid.org/0000-0003-0198-0904
Kejin Wang https://orcid.org/0000-0002-7466-3451
Roberto Braga Figueiredo https://orcid.org/0000-0002-6372-9005